ACS Catalysis

Research Article

Cite This: ACS Catal. 2018, 8, 5621−5629

pubs.acs.org/acscatalysis

Tuning Electronic Push/Pull of Ni-Based Hydroxides To Enhance Hydrogen and Oxygen Evolution Reactions for Water Splitting

Qinghe Zhao,[†] Jinlong Yang,[†] Mingqiang Liu, Rui Wang, Guangxing Zhang, Han Wang, Hanting Tang, Chaokun Liu, Zongwei Mei, Haibiao Chen, and Feng Pan*

School of Advanced Materials, Peking University, Shenzhen Graduate School, Shenzhen 518055, People's Republic of China

Supporting Information

ABSTRACT: Enhancing the efficiency of non-noble electrocatalysts in hydrogen evolution reaction (HER) and oxygen evolution reaction (OER) for water splitting remains a challenging task. Herein, we report an electronic push/pull effect of Co and Fe doping on the HER and OER performance of Ni-based hydroxides as revealed by thorough cyclic voltammetry and X-ray photoelectron spectroscopy analysis. A Fe dopant pulls partial electrons from nearby Ni/Co active sites resulting in a higher electron affinity at the Ni/Co sites to facilitate OH^- adsorption and charge transfer from the adsorbed OH^- for OER. In contrast, a Co dopant tends to push its partial electrons to nearby Ni sites and increase the number of lattice O^{2-} as proton adsorption sites, which lead to faster charge transfer for HER. By adjusting the contents of Co/Fe dopants in Ni-based hydroxides, we were able to tune the electronic configuration of the catalyst and to optimize the OER and HER performance specifically. An optimized catalyst with a composition of $Ni_{0.8}Co_{0.1}Fe_{0.1}O_xH_y$ showed excellent OER performance with an overpotential (η) of 239 mV at 10 mA·cm^{-2} and a Tafel slope of 45.4 mV·dec^{-1}. The HER performance was optimized with a catalyst composition of $Ni_{0.9}Co_{0.1}O_xH_y$ and reached an η of 85 mV at 10 mA·cm^{-2} and a Tafel slope of 84.5 mV·dec^{-1}. Overall water splitting with $Ni_{0.8}Co_{0.1}Fe_{0.1}O_xH_y$ as the anode and $Ni_{0.9}Co_{0.1}O_xH_y$ as the cathode was demonstrated at a low potential of 1.58 V at 10 mA·cm^{-2}. Utilizing the electronic push/pull effect by dopant elements provides a new pathway for the design and optimization of the transition hydroxides as HER and OER catalysts.

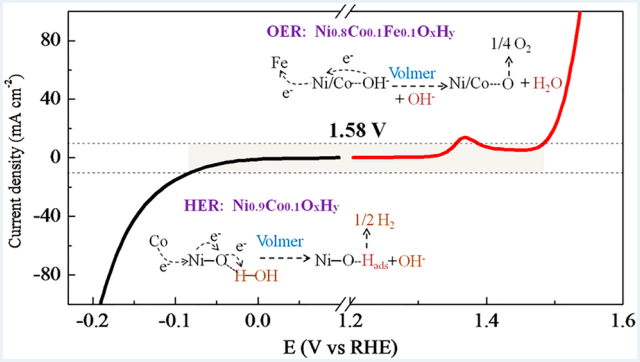

KEYWORDS: *Ni-based hydroxide, electrodeposition, electronic push/pull,water splitting*

INTRODUCTION

The electrochemical water splitting to generate hydrogen and oxygen gases provides a probable pathway to store electricity from renewable sources, and it involves oxygen evolution reaction (OER) and hydrogen evolution reaction (HER).[1−9] However, current commercial electrocatalysts for water splitting still require a potential of 1.8−2.0 V, which is significantly greater than the theoretical 1.23 V.[10−13]The large overpotential (η) is attributed to both the sluggish OER and the facile HER. To minimize the η at both electrodes to improve the efficiency of overall water splitting, novel electrocatalysts with high activity are required and related mechanism needs to be understood. Presently, the outstanding HER and OER catalysts are mostly based on noble metals, such as Pt, Ru, Ir, and their alloys or compounds, which are scarce and costly for application on a large scale.[10−14] Transition metal (M = Fe, Co, Ni, and Mn, etc.) compounds can be the candidate catalysts for overall water splitting, owing to their earth abundance, low-cost, and promising catalytic performance.[15−17] Among them, Ni-based hydroxides are stable and have good electrocatalytic activity toward both OER and HER; thus, the two electrode reactions can be paired together in an integrated electrolytic cell in practical applications.[15−23] For example, a water electrolytic cell was assembled using bifunctional (HER/OER) Fe-doped Ni-based hydroxide electrocatalysts, and it was able to operate at a cell voltage of 1.7 V at 10 mA·cm^{-2} in an alkaline medium, showing attractive performance for practical applications.[12,24]

Multimetallic cation doping was considered to be effective in tuning the electrocatalytic activity at the atomic level.[13,16,17,24−33] In general, mixed metal (Fe, Co, Ni) oxides/hydroxides can exceed corresponding single metal oxides/hydroxides in OER catalysis, possibly owing to altered charge distribution between different metal cations and optimized oxophilicity (e.g., M−OH bond strength), which are believed to facilitate the initialization of OER.[17,29] A typical case is that Fe doping can substantially enhance the OER activity of Ni-based catalysts, but the role of Fe in increasing the OER activity has not been well understood. Boettcher's group[34] found that the conductivity of β-$Ni(OH)_2$ increased by >30-fold upon coprecipitation with Fe, and the increased activity of

Received: April 22, 2018
Published: May 14, 2018

DOI: 10.1021/acscatal.8b01567
ACS Catal. 2018, 8, 5621−5629

β-$Ni_{1-x}Fe_x(OH)_2$ can be attributed to the partial charge transfer activation effect of Fe on Ni. Bates et al.[20,22] revealed that the anodic shift of the precatalytic redox reaction from $Ni(OH)_2$ to NiOOH caused by Fe incorporation was due to the stabilization effect of Fe doping to Ni^{2+} atoms upon more anodic electrode potentials. Friebel et al.[31,35] reported that the active sites for OER in γ-$Ni_{1-x}Fe_xOOH$ were $Ni^{3+/4+}$ and Fe^{3+}, rather than single Ni site, by in situ UV−vis monitoring the solvothermally prepared Ni−Fe(OOH)/C nanoparticles. Conesa et al.[21] showed that Fe doping may induce partial electron shift to Ni in mixed Ni−Fe centers, which stabilizes Ni^{2+} atoms and promotes the formation of Fe^{4+}. Many studies[5,15−17,29] indicated that Co and Fe- codoped Ni-based trimetallic catalyst showed better OER activity than Fe-doped Ni-based bimetallic catalyst, but there is insufficient understanding on the OER mechanism of these trimetallic catalysts. Changing Co/Mn or Co/Fe ratio by changing the Co^{3+}/Co^{2+} ratio and the oxygen vacancies or unsaturated coordination of hydroxyls on oxides/hydroxides surface was found to optimize the surface states and improve OER and HER performance,[36,37] but the effect of Co doping on the water electrolysis performance of Ni-based catalyst is rarely reported. Thus, optimizing the OER and HER performance of Co- or/and Fe-doped Ni-based hydroxides to enhance water-splitting efficiency and understanding the related mechanism are interesting subjects.

In this work, we investigated the HER and OER performance of a series of Co- and Fe-doped Ni-based hydroxide catalysts synthesized by electrodeposition. We demonstrated that the electronic push/pull effect of Co and Fe doping can be utilized to enhance the HER and OER performance of the Ni-based hydroxide catalysts in alkaline media. A systematic study showed that the Fe dopants can pull partial electrons from the Ni/Co active sites resulting in increased electron affinity of the Ni/Co sites for OER. In contrast, Co dopants tend to push its partial electrons to the Ni sites and increase the number of lattice O^{2-} as proton adsorption sites, which lead to faster charge transfer for HER. Using this approach, we identified an optimized catalyst for OER with a composition of $Ni_{0.8}Co_{0.1}Fe_{0.1}O_xH_y$, which demonstrated a low η of 239 mV at 10 mA·cm^{-2} and a Tafel slope of 45.4 mV·dec^{-1} in 1 M KOH. Similarly, we identified an optimized catalyst for HER with a composition of $Ni_{0.9}Co_{0.1}O_xH_y$, which demonstrated a η of 85 mV at 10 mA·cm^{-2} and a Tafel slope of 84.5 mV·dec^{-1}. Therefore, the electronic push/pull effect by multimetallic doping can be utilized as a novel tool to develop mixed transition hydroxides as effective electrocatalysts for water splitting.

RESULTS AND DISCUSSION

Change in the surface morphology of the Ni foam after catalyst deposition is shown in Figure 1a. During the electrodeposition experiment, it was observed that the silvery Ni foam gradually turned black, indicating the successful deposition of a coating. SEM images show that the morphologies of the films vary a lot with the Co and Fe doping contents. The NiO_xH_y film has a relatively smooth surface, while the $Ni_{0.9}Co_{0.1}O_xH_y$ film exhibits a coarse and porous morphology with a domain size between 200 and 800 nm (Figure 1b and c). With Fe doping, the $Ni_{0.9}Fe_{0.1}O_xH_y$ film consists of nanospheres with diameters of smaller than 100 nm, and the $Ni_{0.8}Co_{0.1}Fe_{0.1}O_xH_y$ film displays a similar morphology to that of $Ni_{0.9}Fe_{0.1}O_xH_y$ (Figure 1d and e). SEM results indicate that Co- and Fe-doped Ni-based hydroxides exhibit rougher surfaces, which may contribute to higher electrochemical surface areas compared with NiO_xH_y. SEM images of Ni-based hydroxides with different Co and Fe doping contents are shown in Figure S2−S5, and the different morphologies may be attributed to the different solubility of $Co(OH)_2$, $Ni(OH)_2$, and $Fe(OH)_2$ in the electrodeposition solution. EDS analysis of the chemical composition of $Ni_{0.8}Co_{0.1}Fe_{0.1}O_xH_y$ (Figure 1f) shows only Ni and small content of O as EDS collects signals from a depth of ∼1−5 μm from the surface, suggesting that the catalyst film is very thin. The BET surface areas of NiO_xH_y, $Ni_{0.9}Co_{0.1}O_xH_y$, $Ni_{0.9}Fe_{0.1}O_xH_y$, and $Ni_{0.9}Co_{0.1}Fe_{0.1}O_xH_y$ were measured as 44.0, 66.3, 51.4, and 54.4 m^2·g^{-1} (Table S1). The XRD pattern (Figure 1g) of $Ni_{0.8}Co_{0.1}Fe_{0.1}O_xH_y$ shows only the reflection from metallic Ni, suggesting that the hydroxide was amorphous.

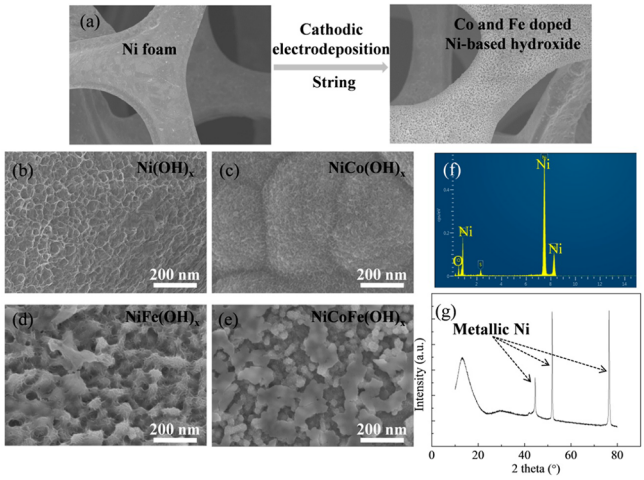

Figure 1. (a) Ni foam before and after electrodeposition of Ni-based hydroxides. SEM images of (b) NiO_xH_y, (c) $Ni_{0.9}Co_{0.1}O_xH_y$, (d) $Ni_{0.9}Fe_{0.1}O_xH_y$, and (e) $Ni_{0.8}Co_{0.1}Fe_{0.1}O_xH_y$. (f) EDS spectrum and (g) XRD spectrum of the $Ni_{0.8}Co_{0.1}Fe_{0.1}O_xH_y$ on Ni foam.

The electrochemically activated OER curves of NiO_xH_y, $Ni_{0.9}Co_{0.1}O_xH_y$, $Ni_{0.9}Fe_{0.1}O_xH_y$, and $Ni_{0.8}Co_{0.1}Fe_{0.1}O_xH_y$ with 80% *iR* corrections in Figure 2a show that both Co and Fe doping can enhance the OER activity of the Ni-based hydroxide catalysts. $Ni_{0.8}Co_{0.1}Fe_{0.1}O_xH_y$ showed the best OER performance with an η of 239 mV at 10 mA·cm^{-2}, while NiO_xH_y exhibited the worst OER performance with an η of 339 mV at 10 mA·cm^{-2}. To evaluate the electron transfer resistance at the catalyst/electrolyte interface, electrical impedance spectroscopy (EIS) was conducted from 100 MHz to 0.1 Hz operating at 0.55 V vs Ag/AgCl (Figure 2b). EIS results show reduced charge transfer resistance (R_{ct}) of hydroxides with Co and Fe doping (3.61, 1.55, 0.50, and 0.34 Ω·cm^2 for NiO_xH_y, $Ni_{0.9}Co_{0.1}O_xH_y$, $Ni_{0.9}Fe_{0.1}O_xH_y$, and $Ni_{0.8}Co_{0.1}Fe_{0.1}O_xH_y$, respectively), and the lowest R_{ct} of $Ni_{0.8}Co_{0.1}Fe_{0.1}O_xH_y$ indicates the fastest charge transfer process. The long-term OER durability tests of the $Ni_{0.8}Co_{0.1}Fe_{0.1}O_xH_y$ hydroxide showed very little decay in performance over 50 h of continuous operation as shown in Figure S14. SEM images of the catalyst (Figure S15) after OER for 50 h further proved its structure stability.

A systematic study on the OER performance of the Ni-based hydroxide catalysts with different Co and Fe doping contents was conducted. The detailed LSV curves, Tafel polarization curves, and fitting curves of the EDLC are illustrated in Figures S6−S8 and Table S3. The kinetic parameters, including η at 10 and 50 mA·cm^{-2}, the Tafel slope, and the EDLC were plotted

DOI: 10.1021/acscatal.8b01567
ACS Catal. 2018, 8, 5621−5629

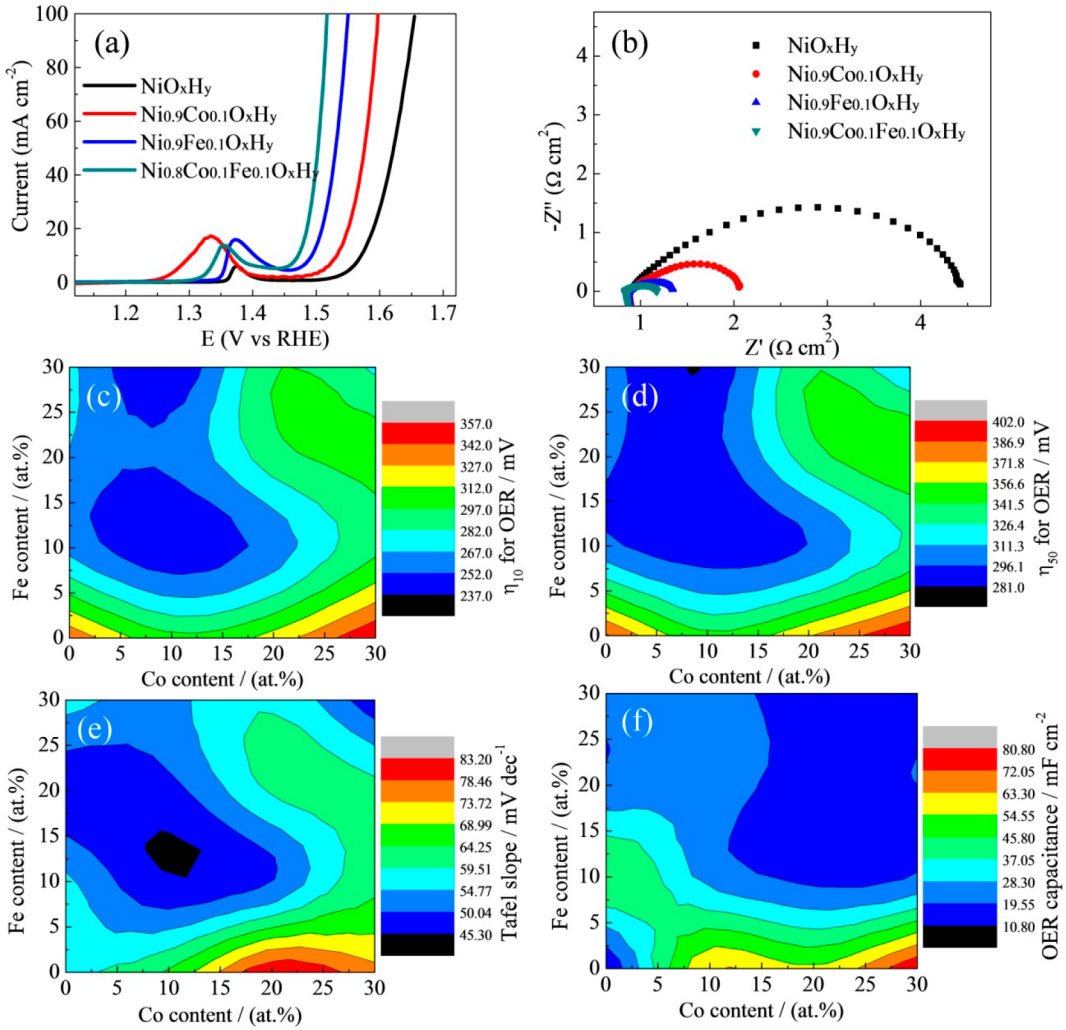

Figure 2. OER performance of Ni-based hydroxides. (a) LSV curves of NiO_xH_y, $Ni_{0.9}Co_{0.1}O_xH_y$, $Ni_{0.9}Fe_{0.1}O_xH_y$, and $Ni_{0.8}Co_{0.1}Fe_{0.1}O_xH_y$ and (b) corresponding EIS plots at potential of 0.55 V vs Ag/AgCl; contour maps of OER kinetic parameters vs Fe and Co fractions of Ni-based hydroxides. (c, d) Overpotentials (η) at 10 and 50 mA cm^{-2}; (e) Tafel slope and (f) OER electric double-layer capacitance representing the electrochemically active surface areas of hydroxides in 1.0 M KOH.

against Co and Fe contents as contour maps for better visualization of the doping effect (Figure 2c–f). The contour maps of η at 10 and 50 mA cm^{-2} and Tafel slope vs Co and Fe contents show a certain degree of consistency. Although at a low content Co doping (<10%) can enhance the OER performance, excess doping by Co may deteriorate the OER performance, while Fe doping can obviously enhance the OER performance. For example, $Ni_{0.7}Co_{0.3}O_xH_y$ shows the worst OER performance with the highest η (357 mV at 10 mA cm^{-2} and 402 mV at 50 mA·cm^{-2}) and the highest Tafel slope (75.5 mV·dec^{-1}), while $Ni_{0.8}Fe_{0.2}O_xH_y$ shows excellent OER performance with η (266 mV at 10 mA·cm^{-2} and 300 mV at 50 mA·cm^{-2}) and Tafel slope (46.4 mV·dec^{-1}). Among all compositions, $Ni_{0.8}Co_{0.1}Fe_{0.1}O_xH_y$ showed the lowest η (239 mV at 10 mA·cm^{-2} and 288 mV at 50 mA·cm^{-2}) and the lowest Tafel slope (45.4 mV·dec^{-1}), which is among the best transition metal hydroxide/oxide catalysts for OER recently reported (Table S3). Besides, we also found that the codoping of Fe and Co in Ni-based hydroxide tends to enhance the OER performance as the Fe/Co ratio ≥1, while it deteriorates the OER activity if the Fe/Co ratio <1. For example, $Ni_{0.8}Co_{0.1}Fe_{0.1}O_xH_y$ exhibited the best OER performance, while $Ni_{0.5}Co_{0.3}Fe_{0.2}O_xH_y$ showed poor OER performance with a high η (303 mV at 10 mA·cm^{-2}) and a high Tafel slope (61.0 mV·dec^{-1}). The contour map of EDLC vs Co and Fe contents (Figure 2f) is notably different from those of η and Tafel slope, suggesting that the EDLC is not directly related to the OER performance in our test. Considering the value of Tafel slopes was in a range from 45.3 to 83.3 mV·dec^{-1}, the charge transfer process from the adsorbed OH^- to the metal active sites is likely the rate-determining step during OER,[38,39] which can be supported by the different contour map of EDLC from those of η and Tafel slope.

A systematic HER study was also conducted using a three-electrode system in 1 M KOH at room temperature. All specimens were electrochemically activated using CV curves before the test to reach a stable state, and 80% *iR* correction was conducted for the measured HER curves (Figure 3a). It can be observed that $Ni_{0.9}Co_{0.1}O_xH_y$ displayed the highest HER performance with the lowest η of 85 mV at 10 mA·cm^{-2}, while $Ni_{0.8}Co_{0.1}Fe_{0.1}O_xH_y$ showed the worst HER performance with a η of 205 mV at 10 mA·cm^{-2}. EIS measurements (Figure 3b) were conducted at HER η of 0.1 V to evaluate the electron transfer resistance at the catalyst/electrolyte interface.

DOI: 10.1021/acscatal.8b01567
ACS Catal. 2018, 8, 5621–5629

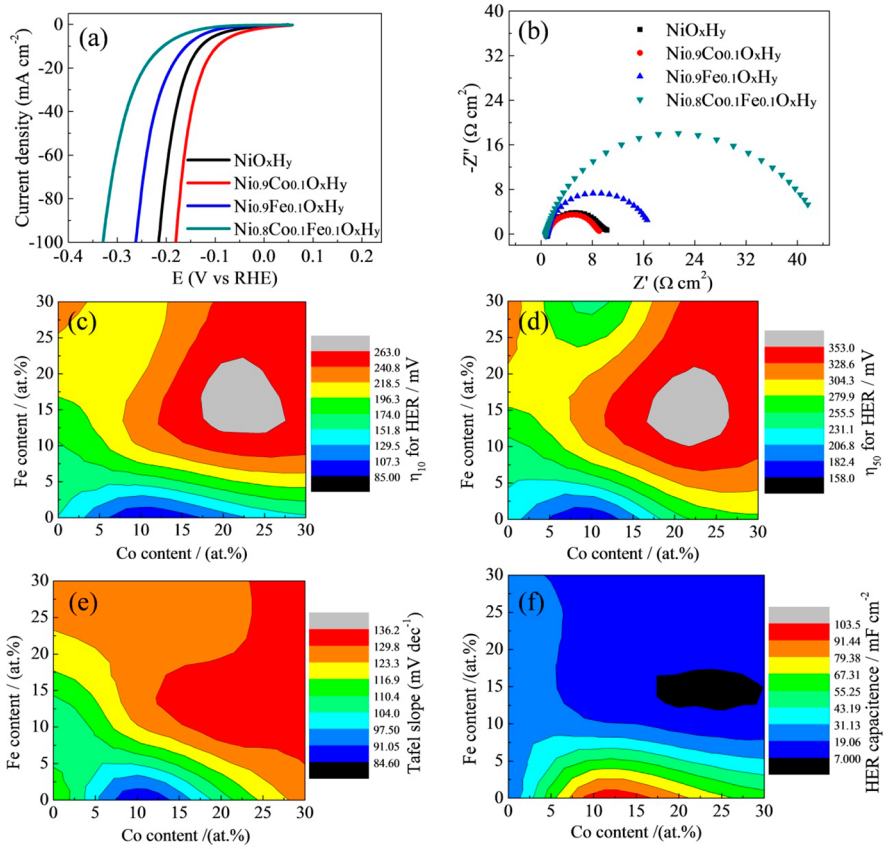

Figure 3. HER performance of the Ni-based hydroxides. (a) HER curves of NiO_xH_y, $Ni_{0.9}Co_{0.1}O_xH_y$, $Ni_{0.9}Fe_{0.1}O_xH_y$, and $Ni_{0.8}Co_{0.1}Fe_{0.1}O_xH_y$, respectively, and (b) corresponding EIS plots at potential of −1.1 V vs Ag/AgCl, (c, d) overpotentials (η) at 10 and 50 mA cm^{-2}, (e) Tafel slope, and (f) electric double layer capacitance (EDLC) of the Ni-based hydroxides vs Co and Fe fractions.

$Ni_{0.9}Co_{0.1}O_xH_y$ exhibited the lowest R_{ct} (3.19 Ω·cm^2), while $Ni_{0.8}Co_{0.1}Fe_{0.1}O_xH_y$ showed an R_{ct} of 41.84 Ω·cm^2 as the highest (Table S5). The HER curves illustrate that Co doping obviously enhances the HER performance, while Fe doping deteriorates the HER performance of our Ni-based hydroxide catalysts in alkaline media. Our $Ni_{0.9}Co_{0.1}O_xH_y$ catalyst is one of the best transition metal oxide/hydroxide catalysts for HER in alkaline media recently reported (Table S6). Besides, the result of long-term HER durability test is shown in Figure S12. The η values of $Ni_{0.9}Co_{0.1}O_xH_y$ for HER were 89 and 163 mV at current densities of 10 and 50 mA·cm^{-2}, respectively; such current densities can be maintained, with little decay, over 50 h of continuous operation, suggesting the high durability of $Ni_{0.9}Co_{0.1}O_xH_y$. In addition, the structural stability of $Ni_{0.9}Co_{0.1}O_xH_y$ is further proved by the SEM images (Figure S14) after HER test for 50 h.

LCV curves for HER were conducted on Ni-based hydroxide catalysts with different Co and Fe doping contents (Figures S9−S11, Table S7). Contour maps of the performance parameters, including η required to reach 10 and 50 mA cm^{-2} (Figure 3c, d) and Tafel slope (Figure 3e), were plotted against dopant contents. The plots show that $Ni_{0.9}Co_{0.1}O_xH_y$ exhibits the best HER performance with the lowest η (85 mV at 10 mA·cm^{-2} and 158 mV at 50 mA·cm^{-2}) and Tafel slope (84.5 mV·dec^{-1}), and $Ni_{0.6}Co_{0.2}Fe_{0.2}O_xH_y$ displayed the highest η (246 mV at 10 mA·cm^{-2} and 353 mV at 50 mA ·cm^{-2}) and Tafel slope (131.6 mV·dec^{-1}). The result indicates that Co doping alone can enhance the HER performance, while Fe doping can deteriorate the HER performance of our Ni-based hydroxide catalysts. The Tafel slope values of the Ni-based hydroxide catalysts were between 80 and 132 mV dec^{-1}. A Talfel slope of ≈120, 40, or 30 mV·dec^{-1} would be expected for the Volmer, Heyrovsky, or Tafel steps, respectively, as the rate-determining step.[41,42] Based on the Tafel slope, the rate-determining step of $Ni_{0.9}Co_{0.1}O_xH_y$ can be both Volmer and Heyrovsky reactions with a Tafel slope of 84.5 mV·dec^{-1}, while Volmer reaction dominates the HER kinetics on $Ni_{0.8}Co_{0.1}Fe_{0.1}O_xH_y$ with a Tafel slope of 123.6 mV·dec^{-1}.[41,42] The Tafel slope difference between $Ni_{0.9}Co_{0.1}O_xH_y$ and $Ni_{0.8}Co_{0.1}Fe_{0.1}O_xH_y$ indicates that $Ni_{0.9}Co_{0.1}O_xH_y$ has more electrochemically active sites for water adsorption and discharge (Volmer) step than $Ni_{0.8}Co_{0.1}Fe_{0.1}O_xH_y$.

The electrochemically active sites for HER were clarified by EDLC. The contour map of EDLC in Figure 3f shows similar trend to those of η and Tafel slope, which suggests that the HER kinetics of these Ni-based hydroxide catalysts are closely related to the electrochemical surface area. For HER, the lower values of η and Tafel slopes are mainly attributed to the higher EDLC of the hydroxides in the alkaline electrolyte. Co doping can dramatically increase the EDLC value of Ni-based hydroxide catalysts. For example, $Ni_{0.9}Co_{0.1}O_xH_y$ exhibited a capacitance value of 103.4 mF·cm^{-2}, which was much higher than that of NiO_xH_y (20.3 mF·cm^{-2}). Fe doping showed nearly no effect on the EDLC of the hydroxide catalysts, and the EDLC values were 27.0, 24.4, and 20.5 mF·cm^{-2} for $Ni_{0.9}Fe_{0.1}O_xH_y$, $Ni_{0.8}Fe_{0.2}O_xH_y$, and $Ni_{0.7}Fe_{0.3}O_xH_y$, respectively. Moreover, codoping of Co and Fe obviously decreases the EDLC value of the catalysts. For instance, $Ni_{0.6}Co_{0.2}Fe_{0.2}O_xH_y$,

DOI: 10.1021/acscatal.8b01567
ACS Catal. 2018, 8, 5621−5629

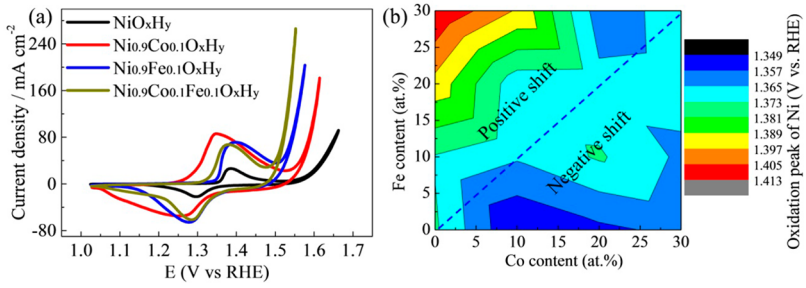

Figure 4. (a) Cyclic voltammetry (CV) curves of the Ni-based hydroxide catalysts and (b) contour map of the potentials vs RHE of oxidation peaks of Ni element, indicating that Fe doping depresses, while Co doping promotes the oxidation process from $Ni(OH)_2$ to NiOOH.

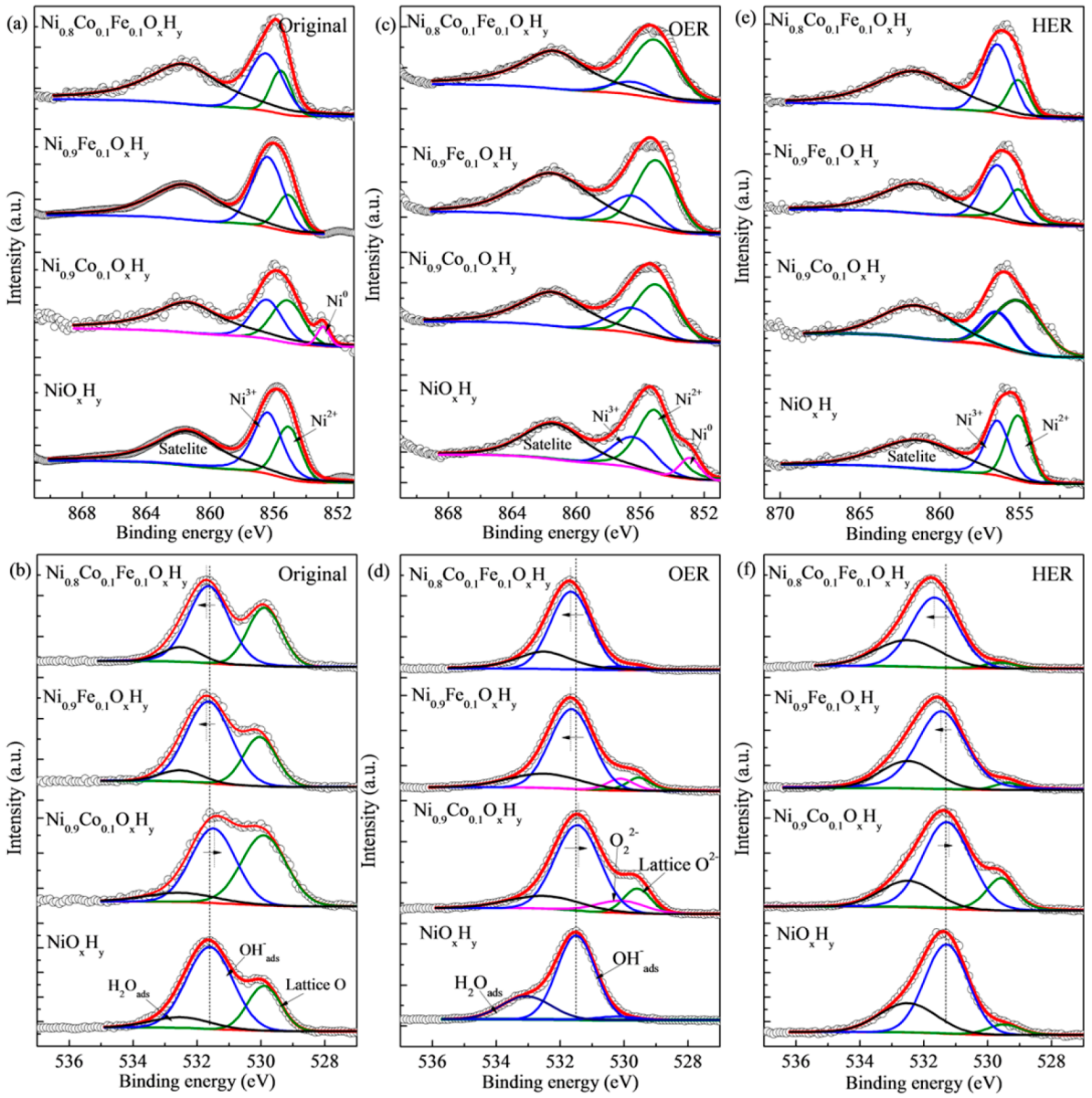

Figure 5. XPS spectra for Ni-based hydroxides at different conditions: (a) Ni 2p and (b) O 1s regions of as-prepared specimens, (c) Ni 2p and (d)O 1s regions after OER tests, and (e) Ni 2p and (f) O 1s regions after HER tests.

$Ni_{0.6}Co_{0.1}Fe_{0.3}O_xH_y$, and $Ni_{0.6}Co_{0.3}Fe_{0.1}O_xH_y$ showed EDLC values of 10.3, 14.9, and 11.0 mF cm^{-2}, respectively. More importantly, we found the activity of Ni active sites was enhanced by the calculations of specific activity (Figure S13). Next, we will prove the electronic push/pull effect of Co/Fe doping to enhance HER/OER performances of Ni-based hydroxides thorough cyclic voltammetry and X-ray photoelectron spectroscopy analysis.

CV measurements were used to investigate the electrochemical precatalytic redox behavior of Ni sites for Co- and Fe-

DOI: 10.1021/acscatal.8b01567
ACS Catal. 2018, 8, 5621−5629

doped Ni-based hydroxide catalysts in 1.0 M KOH. Figure 4a shows the significant differences among NiO_xH_y, $Ni_{0.9}Co_{0.1}O_xH_y$, $Ni_{0.9}Fe_{0.1}O_xH_y$, and $Ni_{0.8}Co_{0.1}Fe_{0.1}O_xH_y$. It can be observed that NiO_xH_y exhibits a reversible redox (1.386/1.298 V for the anodic and cathodic scans), reflecting the transformation between $Ni(OH)_2$ and NiOOH ($Ni(OH)_2 + OH^- \leftrightarrow NiOOH + H_2O + e^-$) in alkaline media.[31,33] With Co doping, the redox peaks of $Ni_{0.9}Co_{0.1}O_xH_y$ negatively shifted to 1.346 and 1.257 V vs RHE for the anodic and cathodic scans, respectively, indicating the promoting effect of Co doping on the oxidation reaction from $Ni(OH)_2$ to NiOOH. Fe doping caused the redox peaks of $Ni_{0.9}Fe_{0.1}O_xH_y$ to be positively shifted to 1.397 and 1.277 V vs RHE for the anodic and cathodic scans, respectively, indicating the depressing effect of Fe doping on the oxidation reaction from $Ni(OH)_2$ to NiOOH. From the above results, Co and Fe doping exert opposite effects on the redox reaction of $Ni(OH)_2$/NiOOH, indicating that the effects of Fe and Co doping on the electronic structure of Ni sites are different, which is reported for the first time. To investigate any synergistic effect of Co and Fe doping on the oxidation behavior of Ni sites in Ni-based hydroxides, the positions of oxidation peaks from $Ni(OH)_2$ to NiOOH were plotted in the form of a contour diagram (Figure 4b). The graph shows the obvious positive shift of the oxidation peaks as the Fe/Co ratio >1.0, and the obvious negative shift of the oxidation peaks if the Fe/Co ratio <1.0, which demonstrates the opposite effect of Co and Fe doping on the oxidation behavior from $Ni(OH)_2$ to NiOOH. The opposite effects of Co and Fe doping on the oxidation behavior from $Ni(OH)_2$ to NiOOH reflect their different effects on the electronic structure of Ni sites, i.e., the electronic push/pull effect of Co/Fe doping, and it contributes to the different OER and HER performance. The electronic push/pull effect of Co/Fe doping can be verified by the XPS results as shown in the following section.

The electronic push/pull of Co and Fe doping can be verified by XPS, and the detailed information on valence and chemical states of Ni 2p and O 1s spectra are presented in Figure 5. The Ni 2p spectra can be fitted with three peaks (Figure 5a), composed of Ni^{2+} peak at binding energy of 855.1 ± 0.1 eV, Ni^{3+} peak at binding energy of 856.4 ± 0.1 eV, and the satellite peak at 861.4 ± 0.1 eV.[5,18,41] We conducted a systematic study on the doping effect of Fe and Co on the valence states of Ni sites in Ni-based hydroxides, which gives a direct evidence for the push/pull effect of Co and Fe doping. The ratio between Ni^{2+} and Ni^{3+} peak areas (Ni^{2+}/Ni^{3+} ratio) was used to evaluate the difference of valence states of Ni element in different catalysts. Although the Ni^{2+}/Ni^{3+} ratio gives a semiquantitative result, it can reflect a trend in the variation of the chemical states of Ni element.

For the as-prepared samples, we observed from Figure 5 that Co doping increased the Ni^{2+}/Ni^{3+} ratio, while Fe doping decreased the Ni^{2+}/Ni^{3+} ratio, indicating that Co dopants push partial electrons to neighboring Ni sites, while Fe dopants pull partial electrons from the neighboring Ni sites. To further verify the push/pull effect of Co and Fe doping on Ni sites, we conducted a systematic study on the dependence of the valence states of Ni sites on the Co/Fe doping contents. With the increasing Co doping content, the values of the Ni^{2+}/Ni^{3+} ratio were 0.623, 1.018, and 3.055 for NiO_xH_y, $Ni_{0.9}Co_{0.1}O_xH_y$, and $Ni_{0.8}Co_{0.2}O_xH_y$, respectively (Figure S18), and 0.390, 0.506, 0.530, and 0.784 for $Ni_{0.9}Fe_{0.1}O_xH_y$, $Ni_{0.8}Co_{0.1}Fe_{0.1}O_xH_y$, $Ni_{0.7}Co_{0.2}Fe_{0.1}O_xH_y$, and $Ni_{0.6}Co_{0.3}Fe_{0.1}O_xH_y$, respectively (Figure S19), which can verify the electronic push effect of Co doping on the valence state of Ni sites. With the increasing Fe doping content, the values of the Ni^{2+}/Ni^{3+} ratio were 0.623, 0.390, and 0.245 for NiO_xH_y, $Ni_{0.9}Fe_{0.1}O_xH_y$, and $Ni_{0.8}Fe_{0.2}O_xH_y$, respectively (Figure S21), and 1.018, 0.506, 0.141, and 0.090 for $Ni_{0.9}Co_{0.1}O_xH_y$, $Ni_{0.8}Co_{0.1}Fe_{0.1}O_xH_y$, $Ni_{0.7}Co_{0.1}Fe_{0.2}O_xH_y$, and $Ni_{0.6}Co_{0.1}Fe_{0.2}O_xH_y$, respectively (Figure S22), which can verify the electronic pull effect of Fe doping on the valence states of Ni sites.

Furthermore, the electronic push/pull of Co and Fe doping can be testified by the binding energy of O 1s spectra. Figure 5b shows the O 1s spectra of as-prepared Ni-based hydroxide catalysts. The O 1s spectra display three pairs of peaks composed of the lattice O^{2-} (529.6 ± 0.1 eV), the adsorbed OH^-(531.3−531.8 eV), and the adsorbed H_2O (532.5 ± 0.1 eV).[40,41] The binding energy of the adsorbed OH^- can reflect the adsorption affinity of OH^- on the Ni sites, which is largely influenced by the electronic push/pull effect of Co and Fe doping. It can be observed that Co doping can decrease the binding energy of the adsorbed OH^-, while Fe doping can increase the binding energy of the adsorbed OH^-. A systematic analysis from Figure S18 to Figure S22 shows that the binding energies of the adsorbed OH^- decrease with the increasing Co doping content in both $Ni_{1-m}Co_mO_xH_y$ and $Ni_{0.9-m}Co_mFe_{0.1}O_xH_y$ and increase with the increasing Fe doping content in both $Ni_{1-n}Fe_nO_xH_y$ and $Ni_{0.9-n}Co_{0.1}Fe_nO_xH_y$. Therefore, we concluded that Co dopants tend to push partial electrons to the neighboring Ni sites, resulting in a higher Ni^{2+}/Ni^{3+} ratio and a lower electron affinity of the Ni sites, and then the binding energy of the adsorbed OH^- decreases. Fe dopants tend to pull partial electrons from the neighboring Ni atoms, resulting in a lower Ni^{2+}/Ni^{3+} ratio and a higher electron affinity of the Ni sites, and then the binding energy of the adsorbed OH^- increases.

The electronic push/pull effects of the Co/Fe doping on OER/HER performances were further investigated by XPS of the catalysts after OER/HER testing. CV curves in Figure 4a show that in the OER region most of Ni activity sites are oxidized to 3+, but the binding energies of Ni 2p in Figure 5c show that there are a great number of Ni^{2+} in the catalysts after OER. The valence of Ni site after OER is closely related to the adsorbed OH^- on the surface, and the charge can transfer from the adsorbed OH^- to the Ni sites. Figure 5d shows the left shift of binding energies of adsorbed OH^- in Fe doping catalysts after OER, which demonstrate that the pull electron effect of Fe doping enhances their OER performance by OH^- adsorption. However, for the single Co doping sample after OER, the obvious lattice O^{2-} on the surface demonstrates the opposite push electron effect is against the OH^- adsorption. EDLC value shows that a weak enhanced OER performance of $Ni_{0.9}Co_{0.1}O_xH_y$ is due to the increase of active sites. Interestingly, we observe that the $Ni_{0.8}Co_{0.1}Fe_{0.1}O_xH_y$ presents higher binding energy of OH^- (left shift) in comparison to $Ni_{0.9}Fe_{0.1}O_xH_y$. For the $Ni_{0.8}Co_{0.1}Fe_{0.1}O_xH_y$, both Ni and Co act as active sites for the adsorption of OH during the OER and HER process. By analyzing Co 2p spectra of $Ni_{0.9}Co_{0.1}O_xH_y$ and $Ni_{0.8}Co_{0.1}Fe_{0.1}O_xH_y$, we find that the Co^{3+}/Co^{2+} ratio increases as the doping of Co in addition to Fe (Figure S23). The results indicate that Co tends to push its partial electrons to Fe sites in $Ni_{0.8}Co_{0.1}Fe_{0.1}O_xH_y$ rather than Ni sites. The generated Co^{3+} may present electronic pull (not push) effect on Ni sites, promote the adsorption of OH, and increase the binding energy of OH (Figure S24). Therefore, $Ni_{0.8}Co_{0.1}Fe_{0.1}O_xH_y$ with Co and Fe codoping processes the

DOI: 10.1021/acscatal.8b01567
ACS Catal. 2018, 8, 5621−5629

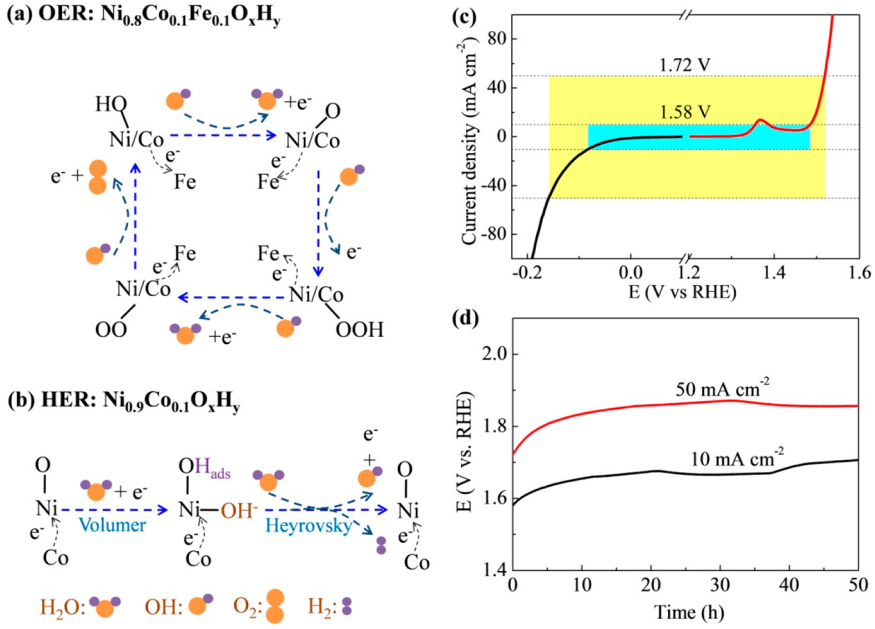

Figure 6. (a) Electronic pull mechanistic schematics of OER process for the $Ni_{0.8}Co_{0.1}Fe_{0.1}O_xH_y$ and (b) electronic push mechanistic schematics of HER process for the $Ni_{0.9}Co_{0.1}O_xH_y$. (c) Potentials of the electrolyzer at 10 and 50 mA·cm^{-2} and (d) long-term durability tests using $Ni_{0.8}Co_{0.1}Fe_{0.1}O_xH_y$ as the cathode and $Ni_{0.9}Co_{0.1}O_xH_y$ as the anode for 50 h in 1 M KOH.

best OER performance because of the double increases of OH^- adsorption and active sites. In addition, for the samples after HER, the Ni^{2+}/Ni^{3+} ratios are similar to those of the as-prepared samples (Figure 5e), but the O 1s binding energies on the surface have changed. Figure 5f shows all OH^- adsorption on the surfaces of Fe doping samples, but the obvious lattice O^{2-} on the surface of $Ni_{0.9}Co_{0.1}O_xH_y$ is attributed to the push electron effect of Co doping, which serves as the adsorption sites of H/H_2O species and promotes the HER performance. The detailed illustrations of electronic push/pull effect of Co/Fe doping on OER/HER are presented in Figure 6a and 6b. Based on the highest HER activity of $Ni_{0.9}Co_{0.1}O_xH_y$ and the highest OER activity of $Ni_{0.8}Co_{0.1}Fe_{0.1}O_xH_y$, thus, we assembled a electrolyzer using $Ni_{0.9}Co_{0.1}O_xH_y$ as cathode and $Ni_{0.8}Co_{0.1}Fe_{0.1}O_xH_y$ as anode for overall water splitting in 1 M KOH. Figure 6c shows that the potentials of the electrolyzer at 10 and 50 mA·cm^{-2} are 1.58 and 1.72 V, respectively, and long-time stability test (Figure 6d) shows that the electrolyzer can be maintained over 50 h of continuous operation at such current densities.

CONCLUSION

In summary, Co and Fe doping exert electronic push/pull effect on the valence state of the Ni sites in the Ni-based hydroxide catalysts and thus influence the OER and HER performance of hydroxides. For OER, Fe doping can pull partial electrons from Ni/Co active sites, which increase the electronic affinity of the Ni and Co sites to the adsorption of OH^- and promotes the charge transfer process from the adsorbed OH^- to the Ni and Co sites and then enhances the OER performance. The $Ni_{0.8}Co_{0.1}Fe_{0.1}O_xH_y$ hydroxide showed the best OER performance with an η of 239 mV at 10 mA·cm^{-2} and a Tafel slope of 45.4 mV·dec^{-1}, and it is one of the best OER catalysts in transition metal hydroxide/oxides. For HER, Co doping pushes its partial electrons to Ni site to promote the charge transfer process from Ni site to the adsorbed H_2O and increase the number of lattice O^{2-} as HER active sites, and then the excellent HER property can be obtained. $Ni_{0.9}Co_{0.1}O_xH_y$ exhibits an η of 85 mV at 10 mA·cm^{-2} and a Tafel slope of 84.5 mV·dec^{-1}, and it is one of the best HER catalysts for transition mental hydroxides/oxides in alkaline media. It is impossible to simultaneously achieve the highest performance in both OER and HER using a single bifunctional catalyst by Co and Fe doping, due to the opposite electronic push/pull effect of Co and Fe doping. We used $Ni_{0.8}Co_{0.1}Fe_{0.1}O_xH_y$ as the cathode and the $Ni_{0.9}Co_{0.1}O_xH_y$ as the anode for the overall water splitting, and the cell operates at a voltage of 1.58 V at 10 mA·cm^{-2}.

ASSOCIATED CONTENT

Supporting Information

The Supporting Information is available free of charge on the ACS Publications website at DOI: 10.1021/acscatal.8b01567.

Experimental details, SEM images, characteristics of hydroxides, HER and OER performances of hydroxides in the literature, LSV curves, Tafel slopes, EDLCs and long-term durability tests for HER and OER, overall water-splitting testing, and XPS spectra changing with Fe- and Co-doping variations for the Ni-based hydroxides (PDF)

AUTHOR INFORMATION

Corresponding Author

*E-mail: panfeng@pkusz.edu.cn.

ORCID

Feng Pan: 0000-0002-8216-1339

Author Contributions

†Q.Z. and J.Y. contributed equally to this investigation. Q.Z. and J.Y. designed the project and performed the catalyst preparation and tests. M.L., R.W., G.Z., H.W., H.T., C.L., and Z.M. carried out measurements and data analyses. Q.Z., J.Y., M.L., H.C., and F.P. discussed the results, analyzed the data,

DOI: 10.1021/acscatal.8b01567
ACS Catal. 2018, 8, 5621−5629

and drafted the manuscript. All authors reviewed the manuscript.

Notes

The authors declare no competing financial interest.

■ ACKNOWLEDGMENTS

The work was financially supported by the National Natural Science Foundation of China (No. 51602009) China Postdoctoral Science Foundation (2016M600008), National Materials Genome Project (2016YFB0700600), and Shenzhen Science and Technology Research Grant (No. JCYJ20160226105838578).

■ REFERENCES

(1) Gong, M.; Zhou, W.; Kenney, M. J.; Kapusta, R.; Cowley, S.; Wu, Y.; Lu, B.; Lin, M. C.; Wang, D. Y.; Yang, J.; Hwang, B.-J.; Dai, H. Blending Cr_2O_3 into a NiO-Ni electrocatalyst for sustained water splitting. *Angew. Chem., Int. Ed.* **2015**, *54*, 11989−11993.

(2) You, B.; Jiang, N.; Sheng, M.; Gul, S.; Yano, J.; Sun, Y. High-Performance Overall Water Splitting Electrocatalysts Derived from Cobalt-Based Metal-Organic Frameworks. *Chem. Mater.* **2015**, *27*, 7636−7642.

(3) Yu, J.; Li, Q.; Li, Y.; Xu, C. Y.; Zhen, L.; Dravid, V. P.; Wu, J. Ternary Metal Phosphide with Triple-Layered Structure as a Low-Cost and Efficient Electrocatalyst for Bifunctional Water Splitting. *Adv. Funct. Mater.* **2016**, *26*, 7644−7651.

(4) Zhang, G.; Jie, Y.; Wang, H.; Chen, H.; Yang, J.; Pan, F. Co_3O_4-δ Quantum Dots as a Highly Efficient Oxygen Evolution Reaction Catalyst for Water Splitting. *ACS Appl. Mater. Interfaces* **2017**, *9*, 16159−16167.

(5) Zhu, X.; Tang, C.; Wang, H. F.; Li, B. Q.; Zhang, Q.; Li, C.; Yang, C.; Wei, F. J. Monolithic-structured ternary hydroxides as freestanding bifunctional electrocatalysts for overall water splitting. *J. Mater. Chem. A* **2016**, *A4*, 7245−7250.

(6) Shang, X.; Chi, J. Q.; Lu, S. S.; Dong, B.; Liu, Z. Z.; Yan, K. L.; Gao, W. K.; Chai, Y. M.; Liu, C. G. Hierarchically three-level $Ni_3(VO_4)_2$@$NiCo_2O_4$ nanostructure based on nickel foam towards highly efficient alkaline hydrogen evolution. *Electrochim. Acta* **2017**, *256*, 100−109.

(7) Dong, B.; Zhao, X.; Han, G. Q.; Li, X.; Shang, X.; Liu, Y. R.; Hu, W. H.; Chai, Y. M.; Zhao, H.; Liu, C.G. J. Two-step synthesis of binary Ni−Fe sulfides supported on nickel foam as highly efficient electrocatalysts for the oxygen evolution reaction. *J. Mater. Chem. A* **2016**, *A4*, 13499−13508.

(8) Shang, X.; Yan, K. L.; Lu, S. S.; Dong, B.; Gao, W. K.; Chi, J. Q.; Liu, Z. Z.; Chai, Y. M.; Liu, C. G. Controlling electrodeposited ultrathin amorphous Fe hydroxides film on V-doped nickel sulfide nanowires as efficient electrocatalyst for water oxidation. *J. Power Sources* **2017**, *363*, 44−53.

(9) Li, X.; Han, G. Q.; Liu, Y. R.; Dong, B.; Hu, W. H.; Shang, X.; Chai, Y. M.; Liu, C. G. NiSe@NiOOH Core−Shell Hyacinth-like Nanostructures on Nickel Foam Synthesized by in Situ Electrochemical Oxidation as an Efficient Electrocatalyst for the Oxygen Evolution Reaction. *ACS Appl. Mater. Interfaces* **2016**, *8*, 20057−20066.

(10) Ma, F. X.; Yu, L.; Xu, C. Y.; Lou, X. W. Self-supported formation of hierarchical $NiCo_2O_4$ tetragonal microtubes with enhanced electrochemical properties. *Energy Environ. Sci.* **2016**, *9*, 862−866.

(11) Wang, H.; Lee, H. W.; Deng, Y.; Lu, Z.; Hsu, P. C.; Liu, Y.; Lin, D.; Cui, Y. Bifunctional non-noble metal oxide nanoparticle electrocatalysts through lithium-induced conversion for overall water splitting. *Nat. Commun.* **2015**, *6*, 1−8.

(12) Yu, L.; Zhou, H.; Sun, J.; Qin, F.; Yu, F.; Bao, J.; Yu, Y.; Chen, S.; Ren, Z. Cu nanowires shelled with NiFe layered double hydroxide nanosheets as bifunctional electrocatalysts for overall water splitting. *Energy Environ. Sci.* **2017**, *10*, 1820−1827.

(13) Lu, X.; Zhao, C. Electrodeposition of hierarchically structured three-dimensional nickel-iron electrodes for efficient oxygen evolution at high current densities. *Nat. Commun.* **2015**, *6*, 1−7.

(14) Xia, B. Y.; Yan, Y.; Li, N.; Wu, H. B.; Lou, X. W.; Wang, X. A metal−organic framework-derived bifunctional oxygen electrocatalyst. *Nat. Energy* **2016**, *1*, 15006−9.

(15) Fan, J.; Chen, Z.; Shi, H.; Zhao, G. In situ grown, self-supported iron-cobalt-nickel alloy amorphous oxide nanosheets with low overpotential toward water oxidation. *Chem. Commun.* **2016**, *52*, 4290−4293.

(16) Qian, L.; Lu, Z.; Xu, T.; Wu, X.; Tian, Y.; Li, Y.; Huo, Z.; Sun, X.; Duan, X. Trinary layered double hydroxides as high-performance bifunctional materials for oxygen electrocatalysis. *Adv. Energy Mater.* **2015**, *5*, 1500245−1500251.

(17) Subbaraman, R.; Tripkovic, D.; Chang, K. C.; Strmcnik, D.; Paulikas, A. P.; Hirunsit, P.; Chan, M.; Greeley, J.; Stamenkovic, V.; Markovic, N. M. Trends in activity for the water electrolyser reactions on 3d M(Ni,Co,Fe,Mn) hydr(oxy)oxide catalysts. *Nat. Mater.* **2012**, *11*, 550−557.

(18) Wang, H. Y.; Hsu, Y. Y.; Chen, R.; Chan, T. S.; Chen, H. M.; Liu, B. Ni^{3+}-Induced Formation of Active NiOOH on the Spinel Ni−Co Oxide Surface for Efficient Oxygen Evolution Reaction. *Adv. Energy Mater.* **2015**, *5*, 395−417.

(19) Yin, J.; Zhou, P.; An, L.; Huang, L.; Shao, C.; Wang, J.; Liu, H.; Xi, P. Self-supported nanoporous $NiCo_2O_4$ nanowires with cobalt-nickel layered oxide nanosheets for overall water splitting. *Nanoscale* **2016**, *8*, 1390−1400.

(20) Chen, J. Y. C.; Dang, L.; Liang, H.; Bi, W.; Gerken, J. B.; Jin, S.; Alp, E. E.; Stahl, S. S. Operando analysis of NiFe and Fe oxyhydroxide electrocatalysts for water oxidation: detection of Fe^{4+} by Mössbauer spectroscopy. *J. Am. Chem. Soc.* **2015**, *137*, 15090−15093.

(21) Görlin, M.; Ferreira de Araujo; Chernev, P.; Reier, T.; Dresp, S.; Paul, B.; Krähnert, R.; Dau, H.; Strasser, P. Oxygen evolution reaction dynamics, faradaic charge efficiency, and the active metal redox states of Ni-Fe oxide water splitting electrocatalysts. *J. Am. Chem. Soc.* **2016**, *138*, 5603−5614.

(22) Görlin, M.; Ferreira de Araujo, J.; Schmies, H.; Bernsmeier, D.; Dresp, S.; Gliech, M.; Jusys, Z.; Chernev, P.; Kraehnert, R.; Dau, H.; Strasser, P. Tracking catalyst redox states and reaction dynamics in Ni-Fe oxyhydroxide oxygen evolution reaction electrocatalysts: the role of catalyst support and electrolyte pH. *J. Am. Chem. Soc.* **2017**, *139*, 2070−2082.

(23) Hou, Y.; Lohe, M. R.; Zhang, J.; Liu, S.; Zhuang, X.; Feng, X. Vertically Oriented Cobalt Selenide/NiFe Layered-Double-Hydroxide Nanosheets Supported on Exfoliated Graphene Foil: An Efficient 3D Electrode for Overall Water Splitting. *Energy Environ. Sci.* **2016**, *9*, 478−483.

(24) Jia, Y.; Zhang, L.; Gao, G.; Chen, H.; Wang, B.; Zhou, J.; Soo, M. T.; Hong, M.; Yan, X.; Qian, G.; Zou, J.; Du, A.; Yao, X. Heterostructure coupling of exfoliated Ni−Fe hydroxide nanosheet and defective graphene as a bifunctional electrocatalyst for overall water splitting. *Adv. Mater.* **2017**, *29*, 1700017−1700025.

(25) Duan, J.; Chen, S.; Vasileff, A.; Qiao, S. Z. Anion and cation modulation in metal compounds for bifunctional overall water splitting. *ACS Nano* **2016**, *10*, 8738−8745.

(26) Liu, W.; Bao, J.; Guan, M.; Zhao, Y.; Lian, J.; Qiu, J.; Xu, L.; Huang, Y.; Qian, J.; Li, H. Nickel-cobalt-layered double hydroxide nanosheet arrays on Ni foam as a bifunctional electrocatalyst for overall water splitting. *Dalton Trans.* **2017**, *46*, 8372−8376.

(27) Nai, J.; Yin, H.; You, T.; Zheng, L.; Zhang, J.; Wang, P.; Jin, Z.; Tian, Y.; Liu, J.; Tang, Z.; Guo, L. Efficient electrocatalytic water oxidation by using amorphous Ni−Co double hydroxides nanocages. *Adv. Energy Mater.* **2015**, *5*, 1401880−1401887.

(28) Yang, Y.; Fei, H.; Ruan, G.; Xiang, C.; Tour, J. M. Efficient electrocatalytic oxygen evolution on amorphous nickel-cobalt binary oxide nanoporous layers. *ACS Nano* **2014**, *8*, 9518−9523.

(29) Wang, A. L.; Xu, H.; Li, G. R. NiCoFe layered triple hydroxides with porous structures as high-performance electrocatalysts for overall water splitting. *ACS Energy Lett.* **2016**, *1*, 445−453.

DOI: 10.1021/acscatal.8b01567
ACS Catal. 2018, 8, 5621−5629

(30) Liu, Q.; Wang, H.; Wang, X.; Tong, R.; Zhou, X.; Peng, X.; Wang, H.; Tao, H.; Zhang, Z. Bifunctional $Ni_{1-x}Fe_x$ layered double hydroxides/Ni foam electrodes for high-efficient overall water splitting: A study on compositional tuning and valence state evolution. *Int. J. Hydrogen Energy* **2017**, *42*, 5560−5568.
(31) Louie, M. W.; Bell, A. T. An investigation of thin-film Ni−Fe oxide catalysts for the electrochemical evolution of oxygen. *J. Am. Chem. Soc.* **2013**, *135*, 12329−12337.
(32) Ma, W.; Ma, R.; Wang, C.; Liang, J.; Liu, X.; Zhou, K.; Sasaki, T. A superlattice of alternately stacked Ni-Fe hydroxide nanosheets and graphene for efficient splitting of water. *ACS Nano* **2015**, *9*, 1977−1984.
(33) Qiu, Y.; Xin, L.; Li, W. Electrocatalytic oxygen evolution over supported small amorphous Ni-Fe nanoparticles in alkaline electrolyte. *Langmuir* **2014**, *30*, 7893−7901.
(34) Trotochaud, L.; Young, S. L.; Ranney, J. K.; Boettcher, S. W. Nickel-iron oxyhydroxide oxygen-evolution electrocatalysts: the role of intentional and incidental iron incorporation. *J. Am. Chem. Soc.* **2014**, *136*, 6744−6753.
(35) Landon, J.; Demeter, E.; İnoğlu, N.; Keturakis, C.; Wachs, I. E.; Vasić, R.; Frenkel, A. I.; Kitchin, J. R. Spectroscopic characterization of mixed Fe−Ni oxide electrocatalysts for the oxygen evolution reaction in alkaline electrolytes. *ACS Catal.* **2012**, *2*, 1793−1801.
(36) Yan, X.; Tian, L.; Atkins, S.; Liu, Y.; Murowchick, J.; Chen, X. Converting $CoMoO_4$ into CoO/MoO_x for overall water splitting by hydrogenation. *ACS Sustainable Chem. Eng.* **2016**, *4*, 3743−3749.
(37) Liu, P. F.; Yang, S.; Zhang, B.; Yang, H. G. Defect-rich ultrathin cobalt-iron layered double hydroxide for electrochemical overall water splitting. *ACS Appl. Mater. Interfaces* **2016**, *8*, 34474−34481.
(38) Indra, A.; Menezes, P. W.; Sahraie, N. R.; Bergmann, A.; Das, C.; Tallarida, M.; Schmeißer, D.; Strasser, P.; Driess, M. Unification of catalytic water oxidation and oxygen reduction reactions: amorphous beat crystalline cobalt iron oxides. *J. Am. Chem. Soc.* **2014**, *136*, 17530−17536.
(39) Shinagawa, T.; Garcia-Esparza, A. T.; Takanabe, K. Insight on Tafel slopes from a microkinetic analysis of aqueous electrocatalysis for energy conversion. *Sci. Rep.* **2015**, *5*, 1−21.
(40) Li, Y. F.; Selloni, A. Mechanism and activity of water oxidation on selected surfaces of pure and Fe-doped NiO_x. *ACS Catal.* **2014**, *4*, 1148−1153.
(41) Barman, B. K.; Das, D.; Nanda, K. K. Facile and one-step synthesis of free-standing 3D MoS_2-rGO/Mo binder-free electrode for efficient hydrogen evolution reaction. *J. Mater. Chem. A* **2017**, *5*, 18081−18087.
(42) Liu, R.; Zhang, G.; Cao, H.; Zhang, S.; Xie, Y.; Haider, A.; Kortz, U.; Chen, B.; Dalal, N. S.; Zhao, Y.; et al. Enhanced proton and electron reservoir abilities of polyoxometalate grafted on graphene for high-performance hydrogen evolution. *Energy Environ. Sci.* **2016**, *9*, 1012−1023.

DOI: 10.1021/acscatal.8b01567
ACS Catal. 2018, 8, 5621−5629